**Adsorption experiments of aerosol-phase $H_2O_2$ on Teflon filters**

It is apparent that $H_2O_2$ is a polar molecule with hydrogen bond, and it has the advantage of strong oxidation. So $H_2O_2$ stands a good chance at adsorbing on the filters. To evaluate the amount of $H_2O_2$ adsorbed on the particle-free Teflon filters, we collected 18 adsorption samples in nine days using the second filter placed after the first filter. The particle-trapped efficiency in the first filter was close to ~ 100 %, thereby avoiding the adsorption interference from aerosols. Half of the samples had no detectable $H_2O_2$, while the concentration of $H_2O_2$ in other samples varied from 0.01 μM to 0.03 μM in the extracted solution of 10 mL $H_3PO_4$, as shown in Fig. S1. The average of all the adsorption samples was about 0.01 μM, accounting for 15 % of measured aerosol-phase $H_2O_2$ concentration. The adsorption experiments verify that $H_2O_2$ is originated from aerosols, rather than from reactions between ambient air species with the filters (Hewitt and Kok, 1991).

**Calculating the residual $H_2O_2$ in raindrops**

$$Sh = 2 + 0.6Re^{1/2}Sc^{1/3} \quad \text{(S1)}$$

$$Sh = \frac{D_P k_g}{D} \quad \text{(S2)}$$

$$Re = \frac{uD_P}{v} \quad \text{(S3)}$$

$$Sc = \frac{v}{D} \quad \text{(S4)}$$

$$C_{aq}^{d} = C_g^m H_A^t - (C_g^m H_A^t - C_{aq}^0)\exp\left(-\frac{6k_g Z}{D_P u H_A^t R T_S}\right) \quad \text{(S5)}$$

Where $D_P$ is the equivalent raindrops diameter, cm; $u$ is the terminal fall velocity of a raindrop, cm $s^{-1}$ (Gunn and Kinzer, 1949); $Sh$ is the Sherwood number, dimensionless; $Re$ is the Reynolds number, dimensionless; $Sc$ is the Schmidt number, dimensionless; $k_g$ is the gas-phase mass transfer coefficient, cm $s^{-1}$ (Adamowicz, 1979); $D$ is the diffusivity of $H_2O_2$ in the air, 0.186 $cm^2$ $s^{-1}$; $v$ is the kinematic viscosity of air, 0.133 $cm^2$ $s^{-1}$; $C_{aq}^{d}$ is the concentration of liquid-phase $H_2O_2$ in

raindrops at the ground (Levine and Schwartz, 1982; Seinfeld and Pandis, 2006), μM; $C_{aq}^{0}$ is the concentration of liquid-phase $H_2O_2$ in raindrops in clouds, μM; $C_g^m$ is the averaged concentration of $H_2O_2$ in the gas phase, $2.98 \times 10^{-10}$ atm; $H_A^t$ is the theoretical Henry's law constant of $H_2O_2$, $8.4 \times 10^4$ M atm$^{-1}$ in pure water at 298 K; $Z$ is the fall distance, m; $R$ is the gas constant, 0.082 L atm K$^{-1}$ mol$^{-1}$, and $T_S$ is the average temperature during rainy days, 298 ± 2 K (mean ± standard deviation, the same hereafter).

**Comparison with $H_2O_2$ level in previous studies**

The average concentration of aerosol-phase $H_2O_2$ in this study was 0.093 ± 0.085 ng μg$^{-1}$, which was a fifth of 0.50 ± 0.30 ng μg$^{-1}$ in Los Angeles (Arellanes et al., 2006) and 0.49 ± 0.55 ng μg$^{-1}$ in Riverside (Wang et al., 2012). Only in one study (Wang et al., 2012), the mean level of $H_2O_2$ in aerosols (0.11 ± 0.07 ng μg$^{-1}$) was close to that in this paper. Details are presented in Table S3. This could be explained as follows.

First, in the studies of Hung and Wang (2001), Venkatachari et al. (2005) and Khurshid et al. (2014), aerosol-phase concentrations of reactive oxygen species (ROS) were measured, including $H_2O_2$, OH radical and other species, thus higher concentrations were observed. In addition, the sonication or ultrasonication methods used were found to produce $H_2O_2$ in purified water, also partially explaining the higher concentrations observed (Arellanes et al., 2006). Second, the extraction time imposed a crucial influence on the concentration of aerosol-phase $H_2O_2$. It has been demonstrated that the concentration of $H_2O_2$ was positively associated with extraction time, due to the decomposition/hydrolysis of several other compounds in the aerosol phase (Hewitt and Kok, 1991; Li et al., 2016). The extraction time in this study was 15 min, compared with 2 h or 4 h in previous studies (Arellanes et al., 2006; Wang et al., 2010; Shen et al., 2011; Wang et al., 2012). We used a shaker to extract the aerosol-phase $H_2O_2$, which has already been confirmed that the extraction efficiency could be up to 97 % with 15 min (Li et al., 2016). Thus, the extraction time should be short to avoid the decomposition/hydrolysis of certain compounds (e.g., organic peroxides) in the aerosol

phase to form additional of $H_2O_2$ in the extracted solution. Third, the concentration of $SO_2$ was higher in China than in the United States. Higher concentration of $SO_2$ may consume more aerosol-phase $H_2O_2$, leading to the lower level of $H_2O_2$ in aerosols in this study. Fourth, pH in aerosols in China was higher than that in the United States, also providing part of explanations to the lower level of aerosol-phase $H_2O_2$ in China, because $H_2O_2$ could be easily decomposed in the weak acid condition (Liu et al., 2017).

**Calculating the contribution of aerosol-phase $H_2O_2$ to sulfate formation in a severe haze event**

We used the thermodynamic model ISORROPIA-II (Guo et al., 2015) to estimate aerosol water content (AWC) based on RH, temperature, the measured cations ($Na^+$, $NH_4^+$, $K^+$, $Mg^{2+}$, and $Ca^{2+}$), and anions ($Cl^-$, $NO_3^-$, and $SO_4^{2-}$) levels. The RH during BJ-2018Winter (5−35 %) was lower than that of previous studies. Because the thermodynamic model ISORROPIA-II has large errors at low RH (Bian et al., 2014), so we calculated AWC during haze events accompanied by high RH, e.g., a heavy haze episode from 2 January to 3 January 2019.

To our knowledge, there are numerous oxidants in the fast growth of $SO_4^{2-}$ on haze days, including $H_2O_2$, $O_3$, transition metals, ROOH, and so on. $H_2O_2$, as a major oxidant in acidic conditions (Hoffmann and Edwards, 1975), has great opportunities to oxidize $SO_2$ into $SO_4^{2-}$ during heavy haze pollution. Because the level of aerosol-phase $H_2O_2$ is higher than the predicted value using gas-aerosol partitioning, we should pay more attention to the measured level of $H_2O_2$ in the aerosol phase, and reevaluate the important contribution of $H_2O_2$ to $SO_4^{2-}$ formation. We calculate the reaction rate (RR) and the sulfate formation rate (SFR) during a heavy haze episode. Given that pH was around 5 in aerosols consistent with recent studies (Liu et al., 2017; Ye et al., 2018), the results are listed in Table S4.

In this study, during a heavy haze episode from 2 January to 3 January 2019, the average level of $SO_2$ was 6.74 ppbv, and the levels of field-measured $H_2O_2$ in the gas and aerosol phases were 16.94 pptv and $6.87 \times 10^3$ μM, respectively. Based on the measured $H_2O_2$,

the mean RR and SFR were around 3.03 × $10^{-3}$ μmol $m^{-3}$ $h^{-1}$ and 0.29 μg $m^{-3}$ $h^{-1}$, which were three orders of magnitude higher than calculated by predicted $H_2O_2$. Moreover, the growth rate of $SO_4^{2-}$ calculated was 0.51 μg $m^{-3}$ $h^{-1}$, and the $H_2O_2$ oxidation pathway contributed to about 57 % of the measured growth of $SO_4^{2-}$. The result strongly suggested that $H_2O_2$ acted as the main oxidant in the formation of sulfate, and might play vital roles in the rapid growth of $PM_{2.5}$ during sever haze pollution.

In this study, the ratio of mass concentration of $SO_4^{2-}$ to $PM_{2.5}$ was 6 %, which was lower than that in previous studies. The ratio in Beijing was 19 % in 2013 (Ho et al., 2016), and decreased to around 10 % in 2016–2017 (Shao et al., 2018; Xu et al., 2019). We suggested that the continued decline of the ratio in 2018 was due to the strict control of $SO_2$ emissions. As a matter of fact, $NO_3^-$ gradually dominated the mass concentration of $PM_{2.5}$ (Xu et al., 2019). Next, the analysis method of $SO_4^{2-}$ in this paper was offline filter-based measurement. The method had a good agreement but was lower than the online measurement (Zhang et al., 2019). In addition, the $SO_4^{2-}$ data was the average during the 11.5 h sampling period, which may underestimate the growth rate of $SO_4^{2-}$. All the reasons mentioned could be responsible for the decrease in the ratio of $SO_4^{2-}$ to $PM_{2.5}$.

**Heterogeneous uptake of $H_2O_2$ on aerosols**

$$\gamma = \frac{5.32 \times 10^{-5}}{1 - 0.82 \times (RH/100)^{0.13}} \quad \text{(S6)}$$

$$\gamma = \frac{d[X]_p^{t,h}/dt}{Z} \quad \text{(S7)}$$

$$Z = \frac{1}{4}\omega A_{es}[X]_g \quad \text{(S8)}$$

$$\omega = \sqrt{\frac{8RT_W}{\pi M_X}} \quad \text{(S9)}$$

$$A_{es} = 3.75 \times ln(M_a) + 12.0 \quad \text{(S10)}$$

$$[X]_p^{t,h} = \int_0^t \frac{d[X]_p^{t,h}}{dt} \quad \text{(S11)}$$

Where $\gamma$ is the heterogeneous uptake coefficient, dimensionless; $[X]_p^{t,h}$ is the net heterogeneous uptake of gas-phase $H_2O_2$ on aerosols, molecules; $Z$ is the collision frequency between gas-phase $H_2O_2$ and aerosols' surface, molecules $s^{-1}$; $\omega$ is the average movement rate of gas-phase $H_2O_2$, m $s^{-1}$; $A_{es}$ is the effective reaction area of aerosols, $m^2$; $[X]_g$ is the concentration of gas-phase $H_2O_2$, molecules $m^{-3}$; $M_X$ is the average molar mass of gas-phase $H_2O_2$, kg $mol^{-1}$; $R$ is the ideal gas constant, 8.314 Pa $m^3$ $K^{-1}$ $mol^{-1}$; $T_W$ is the actual temperature, 270 K; $M_a$ is the mass of aerosols, mg. Subsequently, we could figure out the average of heterogeneous uptake of $H_2O_2$ on aerosols based on Eqs. (S6)−(S11) (Wu et al., 2015).

**Calculating the reaction rates between $H_2O_2$ or $O_3$ and S(IV)**

$$-\frac{d[S(IV)]}{dt} = (k_0[SO_2 \cdot H_2O] + k_1[HSO_3^-] + k_2[SO_3^{2-}])[O_3] \quad \text{(S12)}$$

$$-\frac{d[S(IV)]}{dt} = \frac{7.5 \times 10^7 [H^+][HSO_3^-][H_2O_2]}{1 + 13[H^+]} \quad \text{(S13)}$$

Where $k_0$, $k_1$ and $k_2$ are the rate constants of reactions between $O_3$ and S(IV); $[O_3]$ and $[H_2O_2]$ are liquid-phase levels of $O_3$ and $H_2O_2$; $[SO_2 \cdot H_2O]$, $[HSO_3^-]$ and $[SO_3^{2-}]$ are the concentrations of S(IV) species in the liquid phase.

**The influence of transition metals on aerosol-phase $H_2O_2$ level**

It is demonstrated that Fe and Cu (measured using ICP-MS) had less of an impact on the level of $H_2O_2$ (Fig. S6), similar to the results of previous studies (Tummala, 2015). It is suggested that transition metals might not account for the majority of $H_2O_2$ formation in ambient aerosols in Beijing, instead other physical and chemical reactions play major parts in that, as stated in the text.

**Figure caption.**

**Table S1:** Detection rates and concentrations of peroxides in the liquid and gas phases.

**Table S2:** The differences between measured liquid-phase $H_2O_2$ ($C_{aq}^{m}$) and predicted values ($C_{aq}^{t}$) in three types of seven rain events.

**Table S3:** Summary of aerosol-phase $H_2O_2$ concentration in previous studies.

**Table S4:** The estimated averages of reaction rate (RR) and sulfate formation rate (SFR) during a sever haze event on 2−3 January 2019.

**Table S5:** The ratio of the maximum to initial $H_2O_2$ concentration ($C_{max}/C_0$) in the extracted solution and molar concentration ratio of aerosol-phase TPOs to $H_2O_2$ in three types.

**Table S6:** The average values of meteorological parameters, trace gases, $PM_{2.5}$ and TPOs in the three types during BJ-2018Winter.

**Figure S1:** The concentrations of $H_2O_2$ in adsorption and aerosol samples in the extracted solution from 27 December 2018 to 4 January 2019.

**Figure S2:** Concentrations of measured (a) gas-phase and (b) liquid-phase $H_2O_2$ in seven rain episodes during BJ-2018Summer.

**Figure S3:** The variation of effective field-derived Henry's law constant ($H_A^m$) on temperature in seven rain episodes.

**Figure S4:** The relationship between measured liquid-phase $H_2O_2$ level (left axis) or rain intensity (right axis) with time on 1−2 September 2018.

**Figure S5**: Measured concentrations of (a) gas-phase and (b) aerosol-phase $H_2O_2$ during BJ-2018Winter.

**Figure S6:** The dependency of measured $H_2O_2$ concentration on levels of (a) Cu and (b) Fe in aerosols.

**References**

Adamowicz, R. F.: A model for the reversible washout of sulfur-dioxide, ammonia and carbon-dioxide from a polluted atmosphere and the production of sulfates in raindrops, Atmos. Environ., 13, 105−121, https://doi.org/10.1016/0004-6981(79)90250-6, 1979.

Arellanes, C., Paulson, S. E., Fine, P. M., and Sioutas, C.: Exceeding of Henry's law by hydrogen peroxide associated with urban aerosols, Environ. Sci. Technol., 40, 4859−4866, https://doi.org/10.1021/es0513786, 2006.

Bian, Y. X., Zhao, C. S., Ma, N., Chen, J., and Xu, W. Y.: A study of aerosol liquid water content based on hygroscopicity measurements at high relative humidity in the North China Plain, Atmos. Chem. Phys., 14, 6417–6426, https://doi.org/10.5194/acp-14-6417-2014, 2014.

Gunn, R. and Kinzer, G. D.: The terminal velocity of fall for water droplets in stagnant air, J. Meteorol., 6, 243−248, https://doi.org/10.1175/1520-0469(1949)006<0243:TTVOFF>2.0.CO;2, 1949.

Guo, H., Xu, L., Bougiatioti, A., Cerully, K. M., Capps, S. L., Hite Jr., J. R., Carlton, A. G., Lee, S.-H., Bergin, M. H., Ng, N. L., Nenes, A., and Weber, R. J.: Fine-particle water and pH in the southeastern United States, Atmos. Chem. Phys., 15, 5211–5228, https://doi.org/10.5194/acp-15-5211-2015, 2015.

Hasson, A. S. and Paulson, S. E.: An investigation of the relationship between gas-phase and aerosol-borne hydroperoxides in urban air, J. Aerosol. Sci., 34, 459−468, https://doi.org/10.1016/S0021-8502(03)00002-8, 2003.

Hewitt, C. N. and Kok, G. L.: Formation and occurrence of organic hydroperoxides in the troposphere: laboratory and field observations, J. Atmos. Chem., 12, 181−194, https://doi.org/10.1007/Bf00115779, 1991.

Ho, K. F., Ho, S. S. H., Huang, R. J., Chuang, H. C., Cao, J. J., Han, Y. M., Lui, K. H., Ning, Z., Chuang, K. J., Cheng, T. J., Lee, S. C., Hu, D., Wang, B., and Zhang, R. J.: Chemical composition and bioreactivity of $PM_{2.5}$ during 2013 haze events in China, Atmos. Environ., 126, 162−170, https://doi.org/10.1016/j.atmosenv.2015.11.055, 2016.

Hoffmann, M. R. and Edwards, J. O.: Kinetics of the oxidation of sulfite by hydrogen peroxide in acidic solution, J. Phys. Chem., 79, 2096−2098, https://doi.org/10.1021/j100587a005, 1975.

Hung, H. F. and Wang, C. S.: Experimental determination of reactive oxygen species in Taipei aerosols, J. Aerosol. Sci., 32, 1201−1211, https://doi.org/10.1016/S0021-8502(01)00051-9, 2001.

Khurshid, S. S., Siegel, J. A., and Kinney, K. A.: Technical Note: particulate reactive oxygen species concentrations and their association with environmental conditions in an urban, subtropical climate, Atmos. Chem. Phys., 14, 6777−6784, https://doi.org/10.5194/acp-14-6777-2014, 2014.

Levine, S. Z. and Schwartz, S. E.: In-cloud and below-cloud scavenging of nitric acid vapor, Atmos. Environ., 16, 1725−1734, https://doi.org/10.1016/0004-6981(82)90266-9, 1982.

Li, H., Chen, Z. M., Huang, L. B., and Huang, D.: Organic peroxides' gas-particle partitioning and rapid heterogeneous decomposition on secondary organic aerosol, Atmos. Chem. Phys., 16, 1837−1848, https://doi.org/10.5194/acp-16-1837-2016, 2016.

Liu, M. X., Song, Y., Zhou, T., Xu, Z. Y., Yan, C. Q., Zheng, M., Wu, Z. J., Hu, M., Wu, Y. S., and Zhu, T.: Fine particle pH during severe haze episodes in northern China, Geophys. Res. Lett., 44, 5213−5221, http://doi.org/10.1002/2017GL073210, 2017.

Seinfeld, J. H. and Pandis S. N.: Atmospheric chemistry and physics: from air pollution to climate change, A Wiley-Interscience Publication, New Jersey, the United States of America, 2006.

Shao, P. Y., Tian, H. Z., Sun, Y. J., Liu, H. J., Wu, B. B., Liu, S. H., Liu, X. Y., Wu, Y. M., Liang, W. Z., Wang, Y., Gao, J. J., Xue, Y. F., Bai, X. X., Liu, W., Lin, S. M., and Hu, G. Z.: Characterizing remarkable changes of severe haze events and chemical compositions in multi-size airborne particles ($PM_1$, $PM_{2.5}$ and $PM_{10}$) from January 2013 to 2016−2017 winter in Beijing, China, Atmos. Environ., 189, 133−144, https://doi.org/10.1016/j.atmosenv.2018.06.038, 2018.

Shen, H., Barakat, A. I., and Anastasio, C.: Generation of hydrogen peroxide from San

Joaquin Valley particles in a cell-free solution, Atmos. Chem. Phys., 11, 753−765, https://doi.org/10.5194/acp-11-753-2011, 2011.

Tummala, S. K.: Investigation of the sources of hydrogen peroxide in ambient particulate matter, Master thesis, California State University, the United States of America, 2015.

Venkatachari, P., Hopke, P. K., Grover, B. D., and Eatough, D. J.: Measurement of particle-bound reactive oxygen species in Rubidoux aerosols, J. Atmos. Chem., 52, 325−326, https://doi.org/10.1007/s10874-005-1662-z, 2005.

Wang, Y., Arellanes, C., Curtis, D. B., and Paulson, S. E.: Probing the source of hydrogen peroxide associated with coarse mode aerosol particles in southern California, Environ. Sci. Technol., 44, 4070−4075, https://doi.org/10.1021/es100593k, 2010.

Wang, Y., Arellanes, C., and Paulson, S. E.: Hydrogen peroxide associated with ambient fine-mode, diesel, and biodiesel aerosol particles in southern California, Aerosol Sci. Tech., 46, 394−402, https://doi.org/10.1080/02786826.2011.633582, 2012.

Wu, Q. Q., Huang, L. B., Liang, H., Zhao, Y., Huang, D., and Chen, Z. M.: Heterogeneous reaction of peroxyacetic acid and hydrogen peroxide on ambient aerosol particles under dry and humid conditions: kinetics, mechanism and implications, Atmos. Chem. Phys., 15, 6851−6866, https://doi.org/10.5194/acp-15-6851-2015, 2015.

Xu, Q. C., Wang, S. X., Jiang, J. K., Bhattarai, N., Li, X. X., Chang, X., Qiu, X. H., Zheng, M., Hua, Y., and Hao, J. M.: Nitrate dominates the chemical composition of $PM_{2.5}$ during haze event in Beijing, China, Sci. Total Environ., 689, 1293−1303, https://doi.org/10.1016/j.scitotenv.2019.06.294, 2019.

Ye, C., Liu, P. F., Ma, Z. B., Xue, C. Y., Zhang, C. L., Zhang, Y. Y., Liu, J. F., Liu, C. T., Sun, X., and Mu, Y. J.: High $H_2O_2$ concentrations observed during haze periods during the winter in Beijing: importance of $H_2O_2$ oxidation in sulfate formation, Environ. Sci. Technol. Lett., 5, 757−763, https://doi.org/10.1021/acs.estlett.8b00579, 2018.

Zhang, B. Y., Zhou, T., Liu, Y., Yan, C. Q., Li, X. Y., Yu, J. T., Wang, S. X., Liu, B. X.,

and Zheng, M.: Comparison of water-soluble inorganic ions and trace metals in $PM_{2.5}$ between online and offline measurements in Beijing during winter, Atmos. Pollut. Res., 10, 1755−1765, https://doi.org/10.1016/j.apr.2019.07.007, 2019.

**Table S1:** Detection rates and concentrations of peroxides in the liquid and gas phases.

| Phases | Peroxides | Mean ± S.D. (μM) | Detection rate (%) |
|---|---|---|---|
| Liquid phase | $H_2O_2$ | 44.12 ± 26.49 | 100 |
| | HMHP[a] | 0.23 ± 0.13 | 42 |
| | MHP[b] | 0.41 ± 0.25 | 78 |
| Gas phase | $H_2O_2$ | 0.30 ± 0.26 | 100 |
| | MHP | 0.34 ± 0.03 | 6 |
| | PAA[c] | 0.02 ± 0.01 | 54 |

[a] HMHP is hydroxymethyl hydroperoxide.

[b] MHP is methyl hydroperoxide.

[c] PAA is peroxyacetic acid.

**Table S2:** The differences between measured liquid-phase $H_2O_2$ ($C_{aq}^m$) and predicted values ($C_{aq}^t$) in three types of seven rain events.

| Types | Date | Rain intensity (mm $h^{-1}$) | Number of samples | Number of samples ($C_{aq}^m > C_{aq}^t$) | $C_{aq}^m$ - $C_{aq}^t$ (μM) |
|---|---|---|---|---|---|
| I[a] | 6 August | 0.9 | 4 | 2 | 4.25 |
| II[a] | 30 August[b] | 2.5 | 5 | 5 | 40.19 |
| | 24 July | 5.2 | 10 | 6 | 7.09 |
| | 1 September | 5.5 | 14 | 9 | 10.49 |
| | 8 August | 6.9 | 7 | 7 | 14.71 |
| III[a] | 25 July | 14.7 | 8 | 8 | 39.00 |
| | 5 August | 22.6 | 4 | 3 | 29.91 |

[a] Types I, II, and III refer to rain intensity < 1 mm $h^{-1}$, 1−10 mm $h^{-1}$, and > 10 mm $h^{-1}$, respectively.

[b] The relationship between rain intensity and $C_{aq}^m$ - $C_{aq}^t$ was abnormal on 30 August, and there may be several reasons influencing the liquid-phase $H_2O_2$ concentration.

**Table S3:** Summary of aerosol-phase $H_2O_2$ concentration in previous studies.

| Region | Time | Aerosol phase $H_2O_2$ | Aerosols diameter | Extraction method | Reference |
|---|---|---|---|---|---|
| Niwot Ridge, Colorado, USA | 24 July−4 August 1989 | < 0.01−10 ng $m^{-3}$ | / | soaking for > 30 min | Hewitt and Kok, 1991 |
| UCLA, Los Angeles, CA, USA | May−August 2001 | 0−13 ng $m^{-3}$ | < 10 μm | gentle agitation for several hours | Hasson and Paulson, 2003 |
| UCLA, Los Angeles, CA, USA | after 6 May 2004 | 0.58 ± 0.30 ng $\mu g^{-1}$ | < 2.5 μm | gentle agitation for 2 h | Arellanes et al., 2006 |
| Freeway, Los Angeles, CA, USA | prior to 6 May 2004 | 0.42 ± 0.30 ng $\mu g^{-1}$ | < 2.5 μm | gentle agitation for 2 h | Arellanes et al., 2006 |
| Upwind Riverside, CA, USA | 2−10 August 2005 | 0.48 ± 0.32 ng $\mu g^{-1}$ | 2.5−10 μm | immersing filters for 2 h | Wang et al., 2010 |
| Downwind Riverside, CA, USA | 23 June− 28 August 2008 | 0.37 ± 0.18 ng $\mu g^{-1}$ | 2.5−10 μm | immersing filters for 2 h | Wang et al., 2010 |
| Fresno, California, USA | 2006−2009 | 0.59 ± 0.32 ng $\mu g^{-1}$ | < 2.5 μm | shaking in the dark for 4 h | Shen et al., 2011 |
| UCR, Riverside, CA, USA | 2−10 August 2005 | 0.95 ± 0.69 ng $\mu g^{-1}$[a] | < 2.5 μm | immersing filters for 2 h | Wang et al., 2012 |
| CRCAES, Riverside, CA, USA | 23 June− 28 August 2008 | 0.49 ± 0.55 ng $\mu g^{-1}$[a] | < 2.5 μm | immersing filters for 2 h | Wang et al., 2012 |
| UCLA, Los Angeles, CA, USA | 2009−2010 | 0.11 ± 0.07 ng $\mu g^{-1}$ | < 2.5 μm | immersing filters for 2 h | Wang et al., 2012 |
| Taipei, China | July−September 2000 | 0.68 ng $\mu g^{-1}$[b] | 0.18−1 μm | ultrasonication for 10 min | Hung and Wang, 2001 |
| Rubidoux, CA, USA | July 2003 | 243 ng $m^{-3}$[b] | / | ultrasonication for 15 min | Venkatachari et al., 2005 |
| Austin, Texas, USA | November 2011 −September 2012 | 42.5 ± 37.4 ng $m^{-3}$[b] | / | sonication for 10 min | Khurshid et al., 2014 |
| Beijing, China | 21 December 2018 −5 January 2019 | 0.093 ± 0.085 ng $\mu g^{-1}$ | < 2.5 μm | shaking in the dark for 15 min | This study |

[a] Samples were sporadically contaminated from Virtual Impactors, thus, the aerosol phase $H_2O_2$ level may be above the actual values.

[b] The values are ROS concentrations. ROS concentrations include other reactive oxygen species besides $H_2O_2$.

**Table S4:** The estimated averages of reaction rate (RR) and sulfate formation rate (SFR) during a sever haze event on 2−3 January 2019.

| $H_2O_2$ level | RR (mol $m^{-3}$ $h^{-1}$) | SFR (μg $m^{-3}$ $h^{-1}$) |
|---|---|---|
| Measured_$H_2O_2$ | $3.03 \times 10^{-9}$ | 0.29 |
| Predicted_$H_2O_2$[a] | $6.28 \times 10^{-12}$ | $6.02 \times 10^{-4}$ |

[a] Predicted_$H_2O_2$ is calculated by Henry's law.

**Table S5:** The ratio of the maximum to initial $H_2O_2$ concentration ($C_{max}/C_0$) in the extracted solution and molar concentration ratio of aerosol-phase TPOs to $H_2O_2$ in three types.

| Samples | Types | Date[a] | $C_{max}/C_0$ | Molar concentration ratio of TPOs/$H_2O_2$ |
|---|---|---|---|---|
| 1 | First type | 29 December _D | 1.56 | 4.78 |
| 2 | | 29 December _N | 1.48 | 5.71 |
| 3 | Second type | 31 December _N | 33.68 | 34.45 |
| 4 | | 1 January _D | 44.76 | 45.67 |
| 5 | Third type | 2 January _D | 1.00 | 44.37 |
| 6 | | 2 January _N | 1.00 | 50.80 |

[a] _D and _N represent samples collected at daytime and nighttime, respectively.

**Table S6:** The average values of meteorological parameters, trace gases, $PM_{2.5}$ and TPOs in the three types during BJ-2018Winter.

| Parameters | Samples 1 and 2[a] | Samples 3 and 4[b] | Samples 5 and 6[c] |
|---|---|---|---|
| T (°C) | 269 | 269 | 271 |
| RH (%) | 14.10 | 26.37 | 30.33 |
| WS (m $s^{-1}$) | 1.96 | 1.33 | 0.50 |
| CO (ppbv) | 300.65 | 647.44 | 1065.88 |
| $SO_2$ (ppbv) | 1.40 | 3.45 | 6.50 |
| NO (ppbv) | 1.19 | 23.84 | 44.80 |
| $NO_2$ (ppbv) | 17.03 | 27.03 | 40.23 |
| $O_3$ (ppbv) | 23.33 | 15.43 | 8.99 |
| $PM_{2.5}$ (μg $m^{-3}$) | 13.45 | 37.30 | 63.11 |
| TPOs (ng $m^{-3}$) | 108.50 | 311.75 | 379.16 |
| TPOs (ng $\mu g^{-1}$) | 6.54 | 8.27 | 5.56 |

[a] Samples 1 and 2 were collected on 29 December 2018.

[b] Samples 3 and 4 were collected on 31 December 2018−1 January 2019.

[c] Samples 5 and 6 were collected on 2 January 2019.

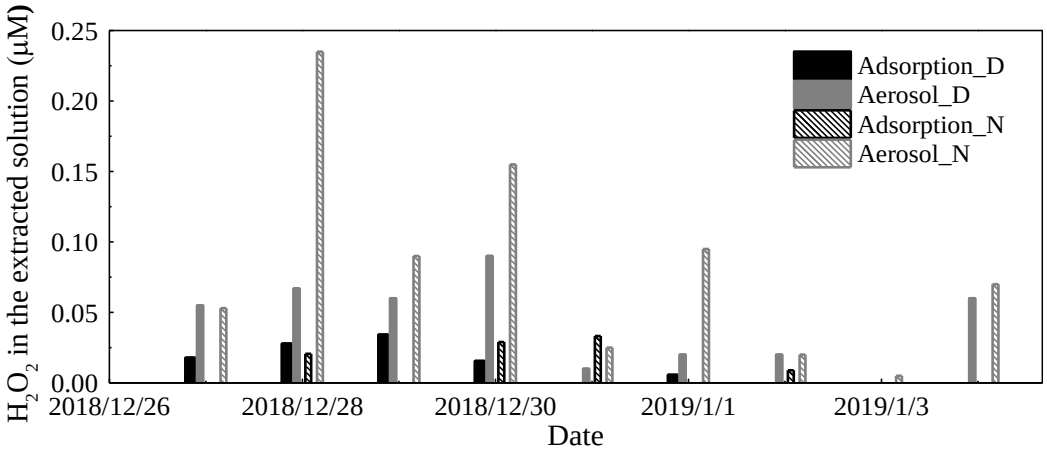


**Figure S1:** The concentrations of $H_2O_2$ in adsorption and aerosol samples in the extracted solution from 27 December 2018 to 4 January 2019. _D and _N denote samples collected at daytime and nighttime, respectively.

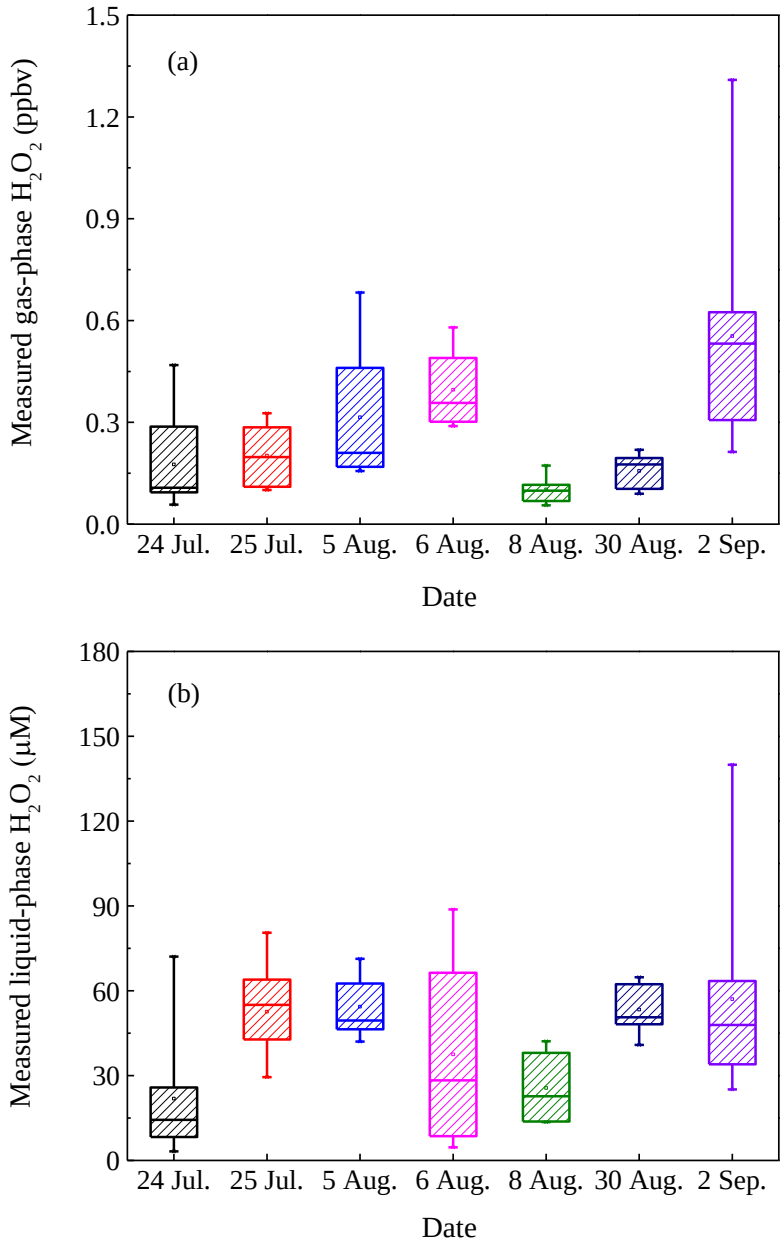


**Figure S2:** Concentrations of measured (a) gas-phase and (b) liquid-phase $H_2O_2$ in seven rain episodes during BJ-2018Summer. Colors represent rain episodes by date. Box ranges represent 25 % and 75 % concentrations of $H_2O_2$, whisker ranges denote minimum and maximum values of $H_2O_2$, and middle square in the box denotes the mean value of $H_2O_2$.

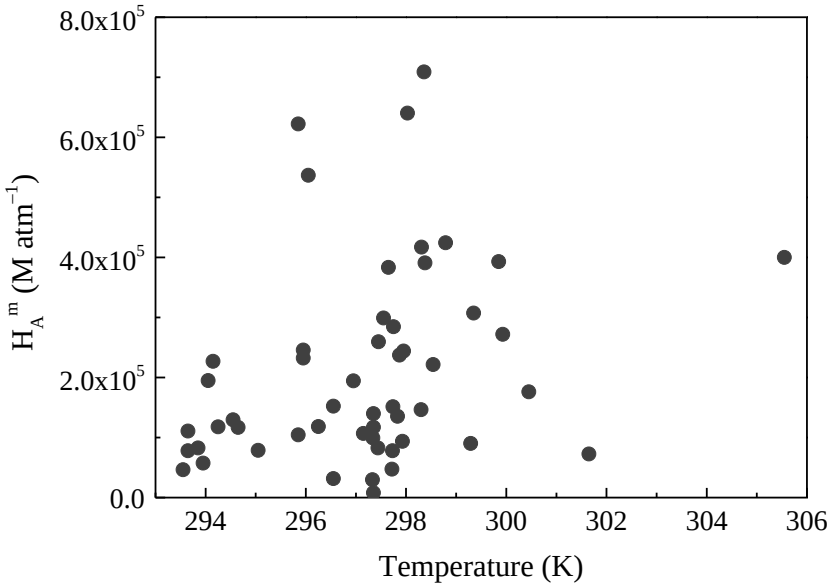


**Figure S3:** The variation of effective field-derived Henry's law constant ($H_A^m$) on temperature in seven rain episodes.

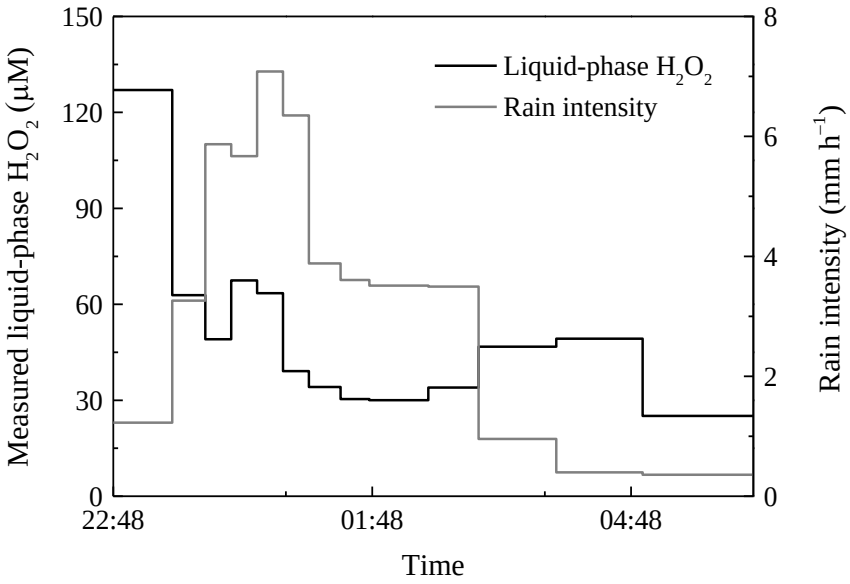


**Figure S4:** The relationship between measured liquid-phase $H_2O_2$ level (left axis) or rain intensity (right axis) with time on 1−2 September 2018.

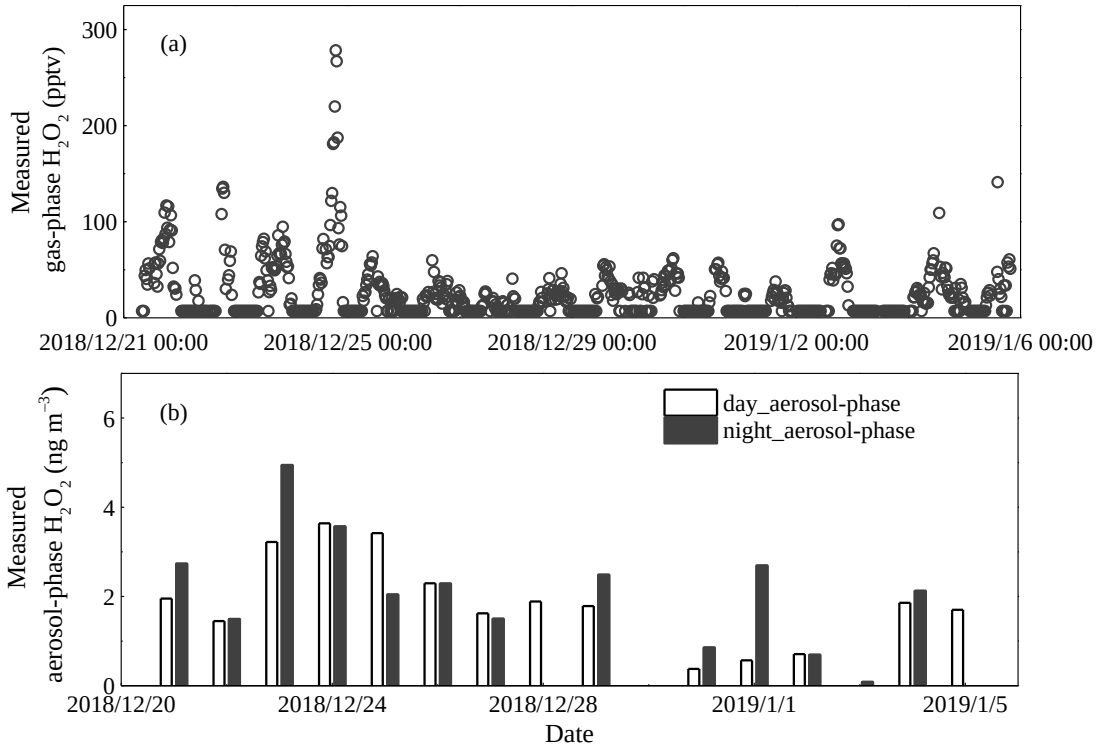


**Figure S5**: Measured concentrations of (a) gas-phase and (b) aerosol-phase $H_2O_2$ during BJ-2018Winter. Day_aerosol-phase and night_aerosol-phase represent samples collected at daytime and nighttime, respectively.

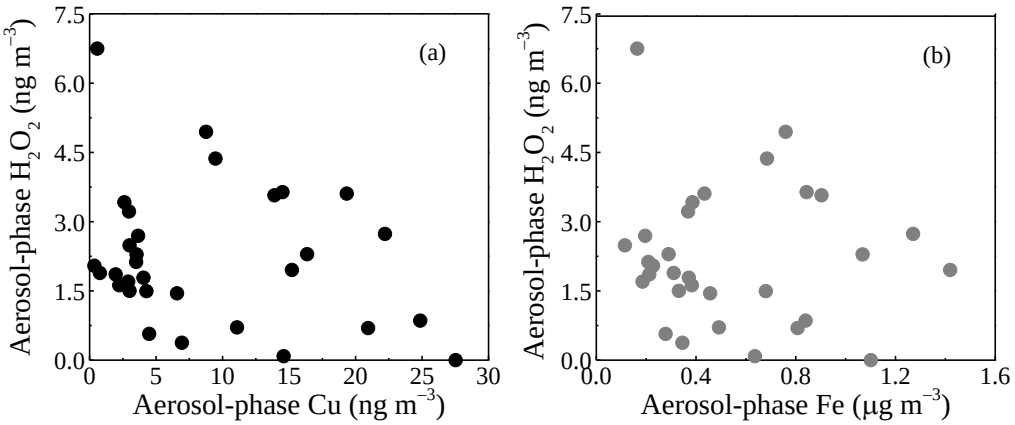


**Figure S6:** The dependency of measured $H_2O_2$ concentration on levels of (a) Cu and (b) Fe in aerosols.